Original Paper

Effect of Depletion and Fluid Injection in the Mesozoic and Paleozoic Sandstone Reservoirs of the October Oil Field, Central Gulf of Suez Basin: Implications on Drilling, Production and Reservoir Stability

Ahmed A. Kassem,[1] **Souvik Sen** ⓘ**,**[2,5] **Ahmed E. Radwan,**[1,3] **Wael K. Abdelghany,**[1] **and Mohamed Abioui**[4]

This work attempted to understand the behavior of the Upper Cretaceous Nezzazat and Lower Cretaceous–Carboniferous Nubia sandstone reservoirs in response to production-induced depletion and fluid injection for enhanced hydrocarbon recoveries from the October oil field, Gulf of Suez, Egypt. Pore pressure (PP), vertical stress (Sv) and minimum horizontal stress (Shmin) magnitudes were modeled based on well logs, drilling data and subsurface measurements. The latest measurements indicated 11.7–12.7 MPa pressure drop (ΔPP) in the Nezzazat reservoirs, while the Nubia sandstone reservoir was depleted by 19–21 MPa. Revised PP and Shmin gradients offer a narrow mud weight window of 9–10.7 PPG (pore pressure gradient) if the entire Lower Miocene–Carboniferous section was planned to be drilled with a single casing in the infill/injector wells. A more conservative approach will be to drill the depleted reservoirs with 5.5–9.3 PPG mud window and case separately, although that may incur an additional cost. Based on the PP–Shmin poro-elastic coupling, stable stress path values of 0.61 and 0.65 are interpreted in the Upper and Lower reservoirs, indicating depletion-induced normal faulting is unlikely to occur at the present rate of depletion. The reservoir stability threshold during pressurization was assessed for fluid injection optimization to sustain production and curtail the bypassed oil. The maximum allowable pressure build-up during injection was estimated using various possible pore pressure–stress coupling scenarios at their maximum depletion state. Based on the PP–Shmin coupling approach, maximum pressure increments of 23 and 27 MPa can be permitted in the depleted Nezzazat and Nubia sandstone reservoirs during injection, without exceeding the lower limit of caprock Shmin, as applicable for both the reservoirs. This will ensure the geomechanical stability of the reservoirs as well as the caprock integrity. This geomechanical study provides crucial comprehensions regarding the optimization of drilling, production, and fluid injection by reducing the risk of reservoir instabilities and formation integrity.

KEY WORDS: In situ stress, Pore pressure, Depletion, Stress path, Fluid injection, Reservoir stability.

[1]Exploration Department, Gulf of Suez Petroleum Company, New Maadi, 2400, Cairo, Egypt.

[2]Geologix Limited, Dynasty Building, Wing A, Level 4, Andheri Kurla Road, Andheri (E), Mumbai, Maharashtra 400059, India.

[3]Faculty of Geography and Geology, Institute of Geological Sciences, Jagiellonian University, Gronostajowa 3a, 30-387 Kraków, Poland.

[4]Department of Earth Sciences, Faculty of Sciences, Ibn Zohr University, 80000 Agadir, Morocco.

[5]To whom correspondence should be addressed; e-mail: souvikseniitb@gmail.com

INTRODUCTION

Depleted hydrocarbon fields require special attention as they possess substantial challenges in terms of production-induced reservoir instability as well as optimum infill/injector drilling design (Soltanzadeh and Hawkes 2007; Fang and Khaskar 2013; Radwan and Sen 2021). If the rate of change of pore pressure (PP) to minimum horizontal stress

(Shmin) exceeds a critical value, it can result in an unstable stress path and induced seismicity (Addis 1997; Chan and Zoback 2002; Haug et al. 2018). Various depleted oil and gas reservoirs across the globe have been characterized by highly unstable stress path values (0.70–1.18) solely resulting from prolonged depletion (Teufel et al. 1991; Winter and King 1991; Addis 1997; Santarelli et al. 1998; Zoback and Zinke 2002; Nelson et al. 2005). Depletion alters the effective downhole drilling mud window; accordingly, casing and mud designs need to be revised in the matured reservoirs. Reservoir pressurization by fluid injection is another critical aspect of such producers, which is a usual practice to sustain production and minimize the bypassed oil. The magnitude of fluid injection should not exceed the critical limit that can cause existing fault slippage at the depleted reservoir intervals during the re-pressurization process (Fang and Khaskar 2010; Safari et al. 2013; Figueiredo et al. 2015; Taghipour et al. 2019). In addition, the pore pressure build-up should not be high enough to induce hydraulic fracturing of the overlying caprock and compromise its geomechanical integrity (Hawkes et al. 2004; Rutqvist et al. 2009; Chiaramonte et al. 2008; Morris et al. 2010; Fang and Khaskar 2013). A comprehensive reservoir geomechanical modeling needs to be implemented to tackle these concerns to achieve drilling and production optimizing by ensuring reservoir stability.

This work attempted to address these key geomechanical challenges in the October oil field, Gulf of Suez Rift Basin. This northernmost megaproducer was discovered during 1970 and 2.38 billion barrels OOIP (original oil in place) was estimated within the Cretaceous and Carboniferous reservoirs (Sercombe et al. 2011; Noureldien and Nabil 2016). Significant literature is available on the geological, drilling and production aspects of this producing giant oil field. El-Ghamri et al. (2002) discussed the hydrocarbon generation and charging in the October field and established that reservoir oil in the October field originated predominantly from the carbonate-rich Sudr Formation. In a recent study, Kassem et al. (2020) correlated the oceanic anoxic event 2 (OAE2) within the Late Cenomanian/Early Turonian organic-rich limestone of the Abu Qada Formation and interpreted its source rock characteristics. A new formation name was formally introduced by Radwan et al. (2020b) as Radwany Formation for the Early–Middle Eocene carbonate sediments by revisiting the sedimentary facies associations and biostratigraphic characteristics. Researchers have communicated good numbers of works on the completion and production engineering issues.

The field started producing from the highly permeable Nezzazat and Nubia sandstone reservoirs in 1977 and reached a peak production of 136,000 BOPD (barrels of oil per day) (EGPC 1996; Askar et al. 2020). The Nezzazat reservoirs were developed at a later stage when the Nubia Formation was in depletion and a slim hole drilling technology was implemented in the development campaign that reduced the drilling cost by 20% (Hassan et al. 2006). To tackle the rapid pressure depletion, the operator engaged water injection by 1996, where the required water was sourced from the Upper Miocene Zeit Formation at around 3000 feet (914.4 m) (Ibrahim et al. 2008). Borling et al. (1996) reported the first successful implementation of the through-tubing bridge plug (TTBP) water shut-off (WSO) workovers that dramatically reduced the water-cut from 55 to 16%. Nassar and Noureldien (2013) performed a reservoir heterogeneity modeling and brought the previously shut-in wells into production which increased production by 1500 BOPD (barrel oil per day). Ibrahim and Mostafa (1999) and Hassan et al. (2006) discussed the production logging problem and downhole integrity management in the October field, respectively. In summary, the reservoir pressure continuously declined further and by 2000, average field production from 49 wells was around 56,000 BOPD with 50% water-cut. Noureldien and Nabil (2016) reported the current production from the October field is around 23,000 BOPD. The present-day water-cut level is around 76% (Askar et al. 2020).

However, none of the previous studies had inferred and documented the effect of depletion and in the future infill development/injector well drilling campaign as well as the critical limit of the water flooding program, which is presently in operation to sustain the reservoir production. This paper is the first geomechanical analysis to address the drilling optimization and reservoir stability aspects. The principal objectives of this work were to: (a) assess the pore pressure and in situ stress perturbations in the producing intervals in response to prolonged depletion; and (b) infer the optimum pore pressure build-up threshold by fluid injection technique to ensure sustainable hydrocarbon production by ensuring reservoir stability and seal integrity. This geomechanical study will assist the operator to
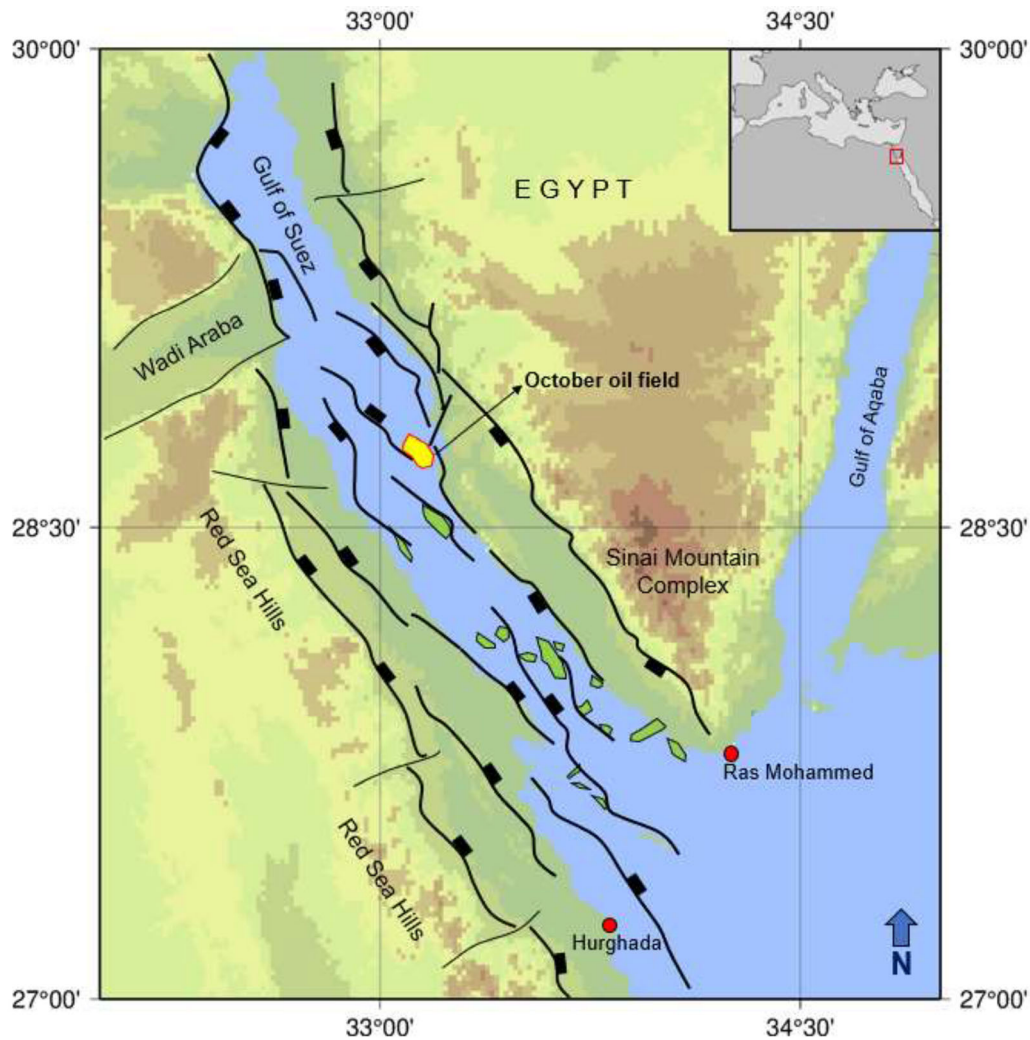
Figure 1. Location of the studied October oil field (yellow polygon) in the Gulf of Suez Rift Basin and other prominent hydrocarbon fields (green polygons). Major structural features and regional extensional faults are marked tentatively (modified after El-Gendy et al. 2017).

optimize the waterflood planning and infill injector drilling.

GEOLOGICAL SETTINGS

The Gulf of Suez Basin is one of the major energy provinces in Egypt and Middle East (Al-sharhan 2003; Dolson 2020). Due to its economic significance, multiple studies have been carried out to investigate its structural, stratigraphic, petroleum, petrophysical, geomechanical, and reservoir characteristics (Lyberis 1988; Schutz 1994; Alsharhan and Salah 1995; Bosworth and McClay 2001; Younes and McClay 2002; El Nady 2006; El Nady et al. 2007;

Attia et al. 2015; Abudeif et al 2016a, b; Attia et al. 2017; Nabawy and El Sharawy 2018; Abudeif et al. 2018; Sallam et al. 2019; Radwan et al. 2019a, b, c, d; Kassem et al. 2020; Radwan et al. 2020c, d; Radwan 2021; Abdelghany et al. 2021; Kassem et al. 2021; Radwan et al. 2021a, b). The October oil field is situated in the Belayim province of the Central Gulf of Suez Basin with 28° 46′–28° 57′ N latitudes and 32° 57′–33° 10′ E longitudes (Fig. 1), covering an area of approximately 22 sq. km (EGPC 1996). The oil field is bounded by a major NW–SE striking normal fault at the western end and by numerous smaller westward-dipping faults at the eastern side (El-Ghamri et al. 2002; Kassem 2018). The field hosts a massive 15,000 feet (4572 m) thick sediment

Table 1. Lithostratigraphic succession of the October oil field. The studied wells were drilled till the Nubia Formation

Age	Formation	Dominant lithology	Thickness (ft.)*
Pleistocene	Zaafarana	Conglomerate, Limestone	2000–4000
Pliocene	Warden	Sandstone, Shale	
Unconformity			
Upper Miocene	Zeit	Anhydrite, Shale, Halite, Sandstone	
	South Gharib	Halite, Anhydrite, Shale	
Middle Miocene	Belayim	Anhydrite, Shale, Sandstone	3300–8200
	Kareem	Sandstone, Shale	
Lower Miocene	Rudeis	Sandstone, Shale, Limestone	
	Nukhul	Sandstone, Shale, Limestone	
Unconformity			
Eocene	Thebes	Limestone, Shale	500–1000
Unconformity			
Upper Cretaceous	Sudr	Limestone	
	Brown Limestone	Limestone, source rock	
	Nezzazat Group		
	Matulla	Sandstone, Limestone, with Shale intercalations	3000–4000
	Wata		
	Abu Qada		
	Raha		
Lower Cretaceous—Carboniferous	Nubia	Sandstone reservoir	2200–3000
Unconformity			
Precambrian	Basement	Metamorphic	

*1 ft = 0.3048 m

column of Carboniferous–Pleistocene age, deposited unconformably above the Precambrian metamorphic basement. This structurally trapped field is a complex of rotated fault blocks typical of rift basins worldwide. A northwest-trending normal fault with a throw of approximately 4000 feet (1219.2 m) has trapped the largest of several oil accumulations, which has a 1092 feet (332.8 m) oil column on the up thrown eastern side (Lelek et al. 1992). A regional lithostratigraphy is provided in Table 1.

Upper Cretaceous Sudr and Senonian Brown Limestone Formations are considered to be the principal source rock intervals (Chowdhary and Taha 1987; Kassem et al. 2017), with an average total organic carbon (TOC) of 2.6% (Lelek et al. 1992). Two primary producing reservoir zones were encountered in the studied wells—Upper Cretaceous Nezzazat Group and Lower Cretaceous to Carboniferous Nubia sandstone reservoirs (Ward and McDonald 1979; El-Ghamri et al. 2002; El Sharawy and Nabawy 2016; El-Gendy et al. 2017; Radwan et al. 2020b). The marine/marginal marine Nezzazat Group has a vertical thickness of around 1200 feet (365.8 m) (Kassem et al. 2020) and consists of the Matulla, Wata, Abu Qada and Raha Formations from top to bottom. Initial field development targeted the laterally continuous, highly permeable fluvial sandstones of the Nubia Formation, which

had a massive vertical thickness of 2300–3000 feet (701.0–914.4 m) (EGPC 1996). The Nezzazat Group reservoirs (Matulla, Wata, Raha) were exploited at a later stage when water-cut was experienced in the Nubia reservoir.

MATERIAL AND METHODS

The studied wells were drilled in approximately 190 feet (57.9 m) of water depth and covered around 13,000 feet (3962.4 m) of the Cenozoic to Carboniferous stratigraphy. These wells targeted the hydrocarbon production from two principal clastic reservoirs: Late Cretaceous Nezzazat group of reservoirs and Early Cretaceous to Carboniferous Nubia sandstones. Drilling data (e.g., mud weight, formation integrity test, etc.), wireline logs (gamma-ray, bulk-density, compressional sonic slowness, and caliper), and well reports (e.g., geological summary, well completion reports, etc.) were studied and used in this work. Applied methods are discussed below.

Pore Pressure (PP) Magnitude

Pore fluid trapped in formation porosities greatly affects the horizontal stress magnitude.

Abnormal formation pressure yields have increased the complexity in drilling and non-productive times (Zhang 2011; Sen et al. 2018a, b; Baouche et al. 2020b, c, d). Direct downhole measurements provide the best PP estimates; however, these data are usually recorded only in reservoir intervals (Sen and Ganguli 2019; Sen et al. 2020; Radwan et al. 2020a; Agbasi et al. 2021). Reservoir pressure data were available from the Nezzazat Group and Nubia sandstone reservoirs, which were used to finalize the reservoir pressure gradient. In addition, a series of similar pressure measurements were carried out throughout the production duration, which identified the change of pore pressure magnitude with time and was therefore used to quantify the depletion pattern. The Upper Cretaceous to Pliocene overburden litho-column is dominated by salt, anhydrite and carbonates along with minor shale intervals. Hence, a compaction trend line-based Eaton's method could not be utilized to calculate pore pressure from available sonic and resistivity logs. However, drilling mud weight was employed as a proxy considering downhole fluid pressure overbalance to prevent fluid influxes during drilling (Radwan et al. 2019a, b, c, d; Sen et al. 2019).

Determination of Vertical Stress (Sv)

Being situated in the active normal faulting tectonic settings, vertical stress (Sv) and Shmin are the highest and least principal stress components in the studied October oil field. Sv is the amount of pressure resulting from the litho-column above and it can be estimated as (Plumb et al. 1991):

$$Sv = \int_0^Z RHOB(Z) * g \, dZ \qquad (1)$$

where g is gravitational acceleration (9.8 m/s^2), and RHOB indicates the wireline bulk-density reading available from the studied wells. A density log, being sensitive to the formation lithology, reflects the variation in Sv gradient throughout the stratigraphy (Sen et al. 2017).

Determination of Shmin

In a normal faulting tectonic setting, Shmin is the least principal stress and it denotes the lower limit of the maximum allowable downhole drilling fluid pressure magnitude, beyond which it can in-duce tensile fractures causing fluid loss. For estimation of Shmin, we employed three approaches.

The first approach utilizes the uniaxial strain model to estimate Shmin magnitude (Zhang and Zhang 2017), thus:

$$Shmin = \frac{v}{1-v}(Sv - \alpha PP) + \alpha PP \qquad (2)$$

where α is the Biot's coefficient, which usually varies between 0.85 and 1 (Bale et al. 2008) but in the absence of core-based bulk modulus measurements, we assumed $\alpha = 1$ (Zoback 2007; Zhang 2013; Baouche et al. 2020a; Ganguli and Sen 2020); and v is the static Poisson's ratio, which can be calculated from P and S wave velocities (Vp and Vs, respectively), thus (Khaksar et al. 2009):

$$v = \frac{Vp^2 - 2Vs^2}{2(Vp^2 - Vs^2)} \qquad (3)$$

This model requires the rock elastic parameter (Poisson's ratio) in the calculation and hence reflects the variation of minimum in situ stress magnitude with varying lithology.

The second model uses the effective stress ratio coefficient to calculate Shmin magnitude, as proposed by Mathews and Kelly (1967), thus:

$$Shmin = PP + K(Sv - PP) \qquad (4)$$

where K is the effective stress ratio coefficient, and it infers the ratio of effective Shmin to effective Sv.

The third model follows the frictional faulting theory, which relates the ratio of minimum to maximum horizontal stress components to a function of frictional coefficient (μ), and the equation for normal faulting tectonic regime (Zoback 2007) is:

$$\frac{Sv - PP}{Shmin - PP} \le \left[(\mu^2 + 1)^{0.5} + \mu \right]^2 \qquad (5)$$

We considered a constant value of frictional coefficient (μ) as 0.6 (Zoback and Healy 1984; Townend and Zoback 2000). We utilized Eq. 5 to define the lower limit of Shmin in the studied October oil field.

Effect of Reservoir Depletion and PP–Shmin Coupling

As a result of hydrocarbon production, reservoir pore pressure decreases, which also changes the in situ stress magnitudes. These changes affect near-

wellbore regions immediately and propagate to the far-field with prolonged production-induced depletion (Addis et al. 1994; Addis 1997; Soltanzadeh and Hawkes 2007; Liu and Harpalani 2014; Radwan and Sen 2021). Maximum horizontal stress and pore pressure couplings are anticipated, but difficulties exist in actual measurements (Hillis 2000; Altmann et al. 2010); therefore, in this study, we focused only on the effect of Shmin changes (ΔShmin) in response to depletion (ΔPP). Ignoring the effect of thermal expansion factor (unaffected reservoir temperature) and the lateral compaction possibility (Segall and Fitzgerald 1996; Santarelli et al. 1998; Goulty 2003; Segura et al. 2011), it can be mathematically expressed as (Geertsma 1957, 1966):

$$\Delta \text{Shmin} = \left(\frac{v}{1-2v}\right)\Delta \text{Sv} + \left(\frac{1-2v}{1-v}\right)\alpha\Delta\text{PP} \quad (6)$$

In case of pure uniaxial compaction ($\Delta \text{Sv} = 0$) (Lorenz et al. 1991; Fjær et al. 2008; Olson et al. 2009) and assuming $\alpha = 1$, Eq. 6 can be rewritten as:

$$\left(\frac{\Delta \text{Shmin}}{\Delta \text{PP}}\right) = \left(\frac{1-2v}{1-v}\right) \quad (7)$$

The above ratio is termed as stress path. In a producing reservoir within normal faulting tectonic regime (following the frictional faulting theory), the Coulomb failure criterion, incorporating the depletion effect, can be expressed as:

$$\frac{\text{Sv} - (\text{PP} - \Delta\text{PP})}{(\text{Shmin} - \Delta\text{Shmin}) - (\text{PP} - \Delta\text{PP})} = \left[\sqrt{\mu^2 + 1} + \mu\right]^2$$
$$= f(\mu)$$
$$(8)$$

Equating the rate of change of minimum stress to pore pressure reduction as stress path factor (A), Eq. 8 can be further simplified as (Chan and Zoback 2002):

$$\left(\frac{\Delta \text{Shmin}}{\Delta \text{PP}}\right) = 1 - \frac{1}{\left[\sqrt{\mu^2 + 1} + \mu\right]^2} \quad (9)$$

With $\mu = 0.6$, a normal faulting stress path limit was found to be 0.68. This deciphers that if a stress path value of a producing interval exceeds this critical limit (stress path > 0.68), it can induce production-related normal faulting and make the reservoir geomechanically unstable (Chan and Zoback 2002; Zoback and Zinke 2002).

Effect of Fluid Injection on Reservoir Stability

If the shear stress effective on a pre-existing fault or fracture plane crosses the shear strength, it results in a slip (Zoback 2007). Fault activation potential is another critical aspect of geomechanical modeling to infer the threshold fluid pressure to just maintain the stability of the fault plane, as increased pore fluid pressure during the re-pressurization process reduces the effective normal stress magnitudes considerably (Ganguli et al. 2018). The critical pore fluid pressure (PPc) to induce slip on any randomly positioned fault can be deduced from the Terzaghi (1923) effective stress law and the Coulomb failure criterion (Streit and Hillis 2004; Jaeger et al. 2007). Considering cohesion-less fault situation and coefficient of internal friction as 0.6, it can be expressed as (Figueiredo et al. 2015; Taghipour et al. 2019):

$$\text{PPc} = \frac{3\sigma_3 - \sigma_1}{2} \quad (10)$$

where σ_3 and σ_1 denote the minimum and maximum principal stress components, respectively, and which are Shmin and Sv in the case of the studied October oilfield, respectively. This traditional approach of critical pressure estimation assumes that the total stress distribution is unchanged by the injection or pressurization process and thus ignores the field scale pore pressure-stress coupling phenomenon (Lynch et al. 2013). Recent studies indicated that fluid injection affects the total stresses and induces deformations (Altmann et al. 2010; Schoenball et al. 2010; Vidal–Gilbert et al. 2010; Safari et al. 2013; Kim and Hosseini 2014). In a recent work, Kim and Hosseini (2016) performed numerical modeling to infer pore pressure–stress perturbations during isothermal fluid injection at various reservoir structural geometry and boundary conditions. Considering a homogenous infinite medium, the terminal values of stress vs pore pressure perturbation ratio along the radial and tangential directions can be expressed, respectively, as (Altmann et al. 2010; Vidal-Gilbert et al. 2010; Kim and Hosseini 2016):

$$\text{Radial change} : \left(\frac{\Delta\sigma_{\text{Radial}}}{\Delta\text{PP}}\right) = \alpha\left(\frac{1-2v}{1-v}\right) \quad (11)$$

$$\text{Tangential change} : \left(\frac{\Delta\sigma_{\text{Tangential}}}{\Delta\text{PP}}\right) = \frac{\alpha}{2}\left(\frac{1-2v}{1-v}\right)$$
$$(12)$$

It is critical to determine whether a current fluid injection rate is required to be revised based on the pressure build-up magnitude. In this regard, Kim and Hosseini (2016) suggested a guideline that provides a more precise characterization of the injection stress path. They advised using Eq. 11 in the radial direction for inside an injection zone as well as for the interface between the injection zone and caprock to update the stress with a given estimate of pore-pressure build up. In the vertical direction, Kim and Hosseini (2016) recommended adopting $\Delta\sigma z/\Delta P = 0$ for the inside of an injection zone and Eq. 12 at the interface to update the stress. Vilarrasa et al. (2013) deciphered that the change in Sv can be neglected in the middle part of the injection zone ($\Delta Sv/\Delta PP = 0$), whereas it shows higher values in the upper part of the reservoir, specifically at the interface due to the excess pore pressure build-up at the initial injection period since the injected fluid cannot flow into the impermeable caprock. The same observations were also made by Kim and Hosseini (2016) in their analytical modeling. For small size reservoirs with low uniaxial compressive strengths (UCS), 50% of ΔSv can be arched away (Mulders 2003). In a reservoir geomechanical modeling of the depleted Shearwater gas-producing interval of North Sea, Kenter et al. (1998) interpreted a 20–30% Sv arching. Traditionally, effective stress is measured simply with initial total stress (σ_0), pore-pressure ($PP' = PP_0 + \Delta PP$), and Biot's coefficient as $\sigma' = \sigma_0 - \alpha(PP_0 + \Delta PP)$. Considering the pore pressure–stress coupling scenario during injection, the revised effective vertical (σ'_v) and minimum horizontal (σ'_{hmin}) stresses can be expressed, respectively, as:

$$\begin{aligned}\sigma'_v &= \sigma_{v0} + \Delta\sigma_v^P - \alpha PP' \\ &= \sigma_{v0} + \beta_v\Delta PP - \alpha(PP_0 + \Delta PP)\end{aligned} \quad (13)$$

$$\begin{aligned}\sigma'_{hmin} &= \sigma_{h0} + \Delta\sigma_h^P - \alpha PP' \\ &= \sigma_{h0} + \beta_h\Delta PP - \alpha(PP_0 + \Delta PP)\end{aligned} \quad (14)$$

where σ_{v0} and σ_{h0} refer to the initial stress conditions, and $\beta_v = \left(\frac{\Delta\sigma_v}{\Delta PP}\right)$ and $\beta_h = \left(\frac{\Delta\sigma_{hmin}}{\Delta PP}\right)$. β_h and β_v represent the stress vs pore pressure perturbation ratios along the radial and tangential directions, respectively, and are estimated by Eqs. (11) and (12), respectively. If we just consider the coupling between PP and Shmin, with $\Delta Sv = 0$ (absence of Sv arching), it produces $\beta_v = 0$ and $\beta_h > 0$. This sce-

nario is strongly similar to the depletion stress path stated in Eq. 7, which also assumes uniaxial compaction. The traditional constant total stress solutions, as well as pore pressure–stress coupling results, can be plotted in a $\sigma'_v - \sigma'_{hmin}$ cross-plot following the Coulomb failure criterion (Kim and Hosseini 2016) to interpret the maximum allowable pressure that the depleted reservoir can sustain during the waterflood injection.

Effect of Fluid Injection on Caprock Integrity

Fluid injection gradually increases the pore pressure of the depleted interval. If the pore pressure build-up by the re-pressurization process exceeds the fracturing limit of the overlying caprock, it can be hydraulically fractured, and the vertical seal may be lost (Hawkes et al. 2004; Rutqvist et al. 2009; Chiaramonte et al. 2008; Morris et al. 2010; Fang and Khaskar 2013). Therefore, caprock integrity is an important aspect of the fluid injection design to infer the maximum allowable pore pressure increase without inducing geomechanical instability in the top seal. Caprock will experience tensile fracturing if:

$$FP_{Cap} \geq Shmin + TS_{Cap} \quad (15)$$

where FP_{Cap} is the fracture pressure of the caprock, Shmin is the reservoir's minimum horizontal stress, and TS_{Cap} is the tensile strength of the caprock.

RESULTS AND DISCUSSIONS

Pore Pressure and In Situ Stresses in Virgin Condition

Density log-derived Sv provides an average gradient of 21.3 MPa/km (0.94 PSI/ft) in the Carboniferous–Pleistocene stratigraphy of the October oil field (Fig. 2). Lithological distribution is the key factor against the vertical variation of Sv gradient. A formation specific investigation suggests a relative lower Sv gradient of about 20.56 MPa/km (0.90 PSI/ft) in the 21.54 MPa/km (0.95 PSI/ft) was interpreted in the underlying South Gharib and Belayim Formations, which host evaporites (halite and anhydrite) dominantly, and clastics (sandstones and shales) (Fig. 2). The carbonates-dominated Kar-
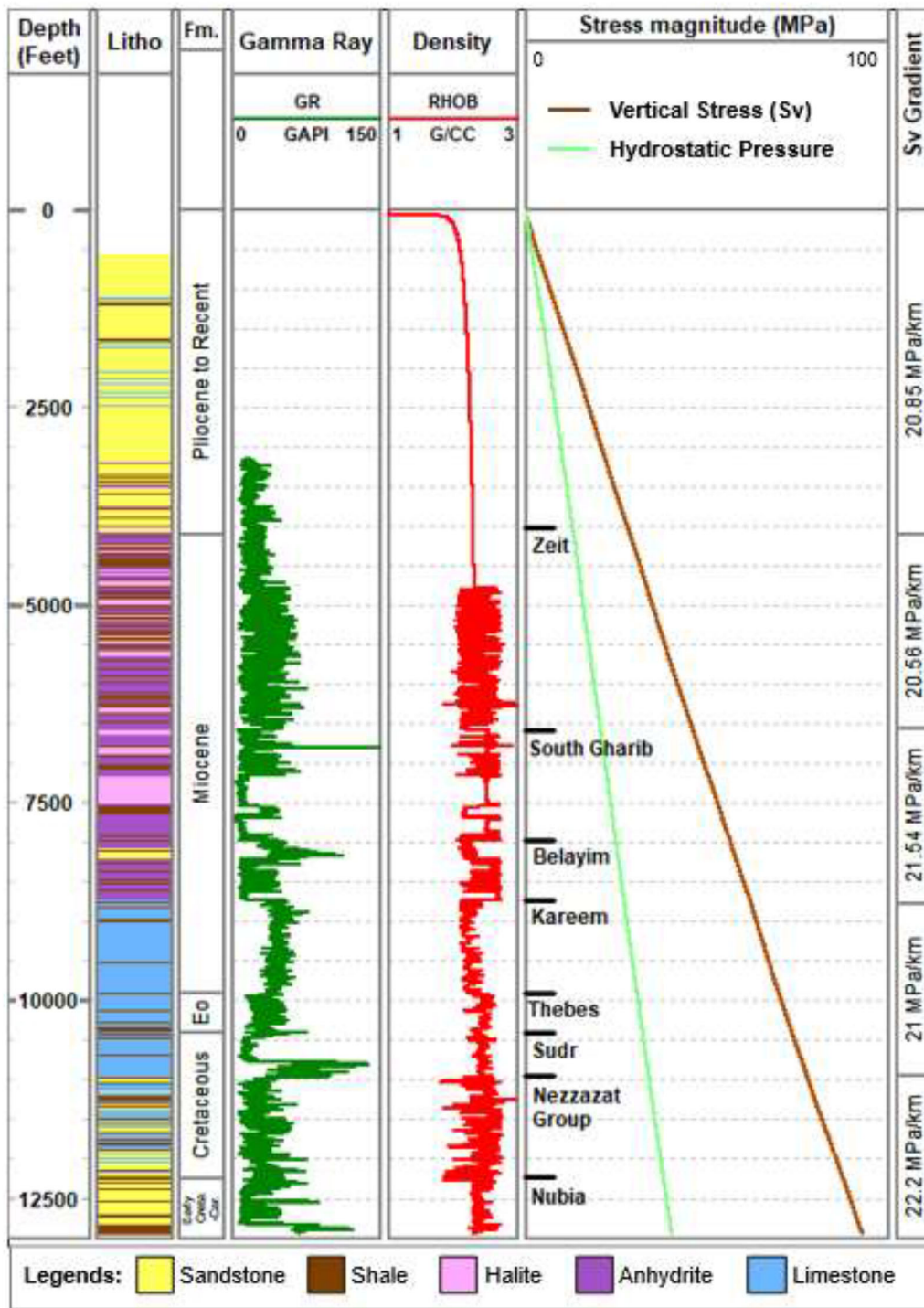
Figure 2. Interpreted vertical stress (Sv) magnitude and gradients across the entire stratigraphy, as encountered in the October oil field.

eem–Rudeis–Nukhul, Eocene Thebes and Upper Cretaceous Sudr Formations exhibit around 21 MPa/km (0.93 PSI/ft) Sv gradient, while the clastic reservoirs successions of the Nezzazat Group and Nubia Formation provided an average Sv gradient of 22.2 MPa/km (0.98 PSI/ft).
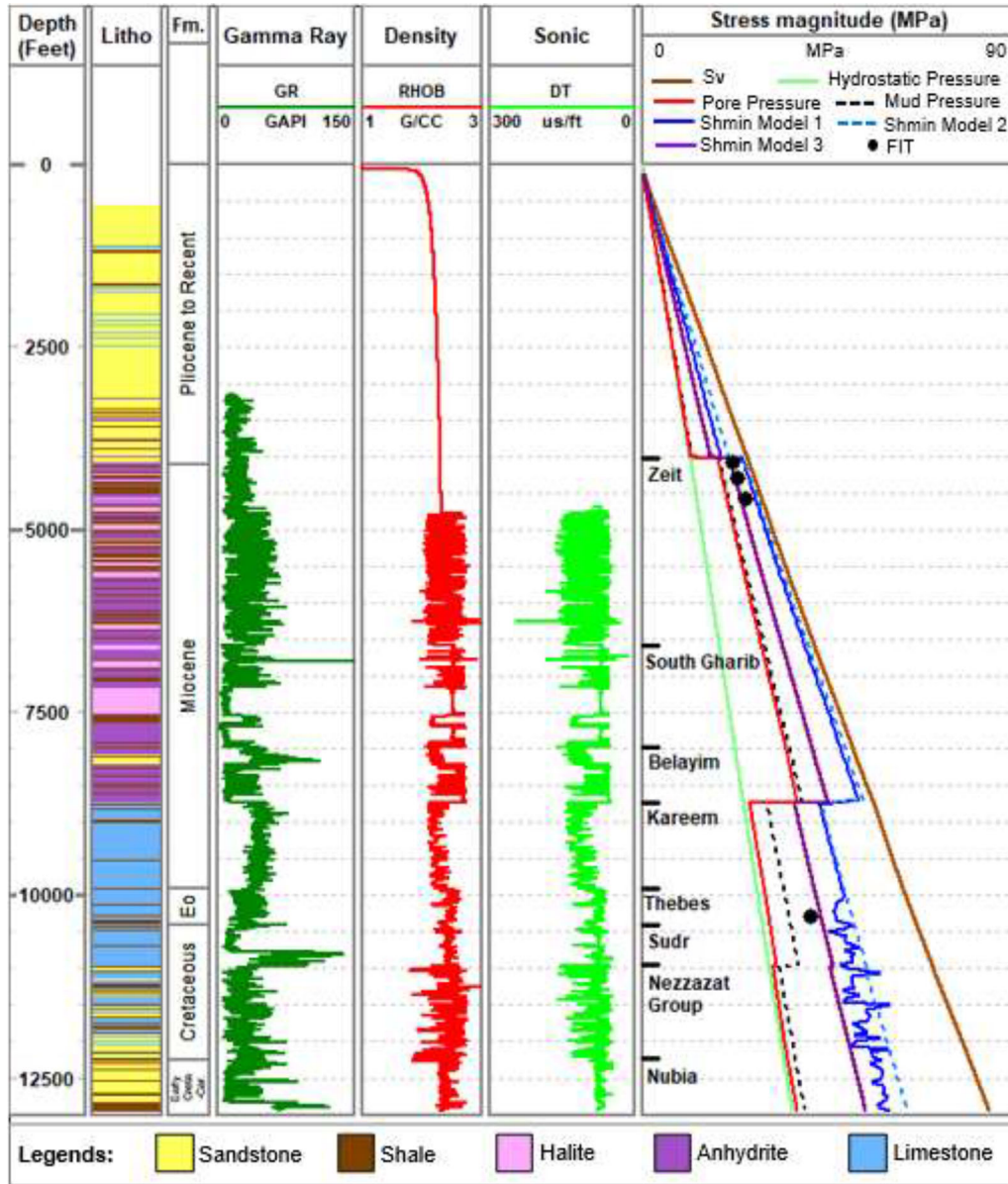
Figure 3. Interpreted PP, Sv and Shmin magnitudes of the Well B2 in the virgin condition. Shmin was estimated by three models: Model 1 = uniaxial strain model (Zhang and Zhang 2017); Model 2 = effective stress ratio model (Mathews and Kelly 1967) and Shmin lower limit by Model 3 = frictional faulting theory (Zoback 2007).

It is to be noted that the studied wells had been drilled in the initial appraisal and expansion stages of the October field development. The virgin reservoir pressure gradients of the Nezzazat Group and Nubia sandstone Formation were interpreted from the earliest possible reservoir pressure measurements dated back to 1980, which provided a PP gradient of 10.14–10.36 MPa/km (0.448–0.458 PSI/ft) (Fig. 3). The non-reservoir overburden was dominated by evaporites (halite, anhydrite) and limestones along with shale intercalations. Based on the mud overbalance proxy, we finalized the pore pressure in those intervals. Halite, due to its plastic nature, was drilled with the highest mud weight, which was assumed as the pressure gradient of the anhydrite bearing formations (Fig. 3) and the value was around 13.6 MPa/km (0.6 PSI/ft). Based on the minimum drilling mud weight used and drilling experiences, the Middle Miocene–Upper Cretaceous carbonates above the top reservoir interval
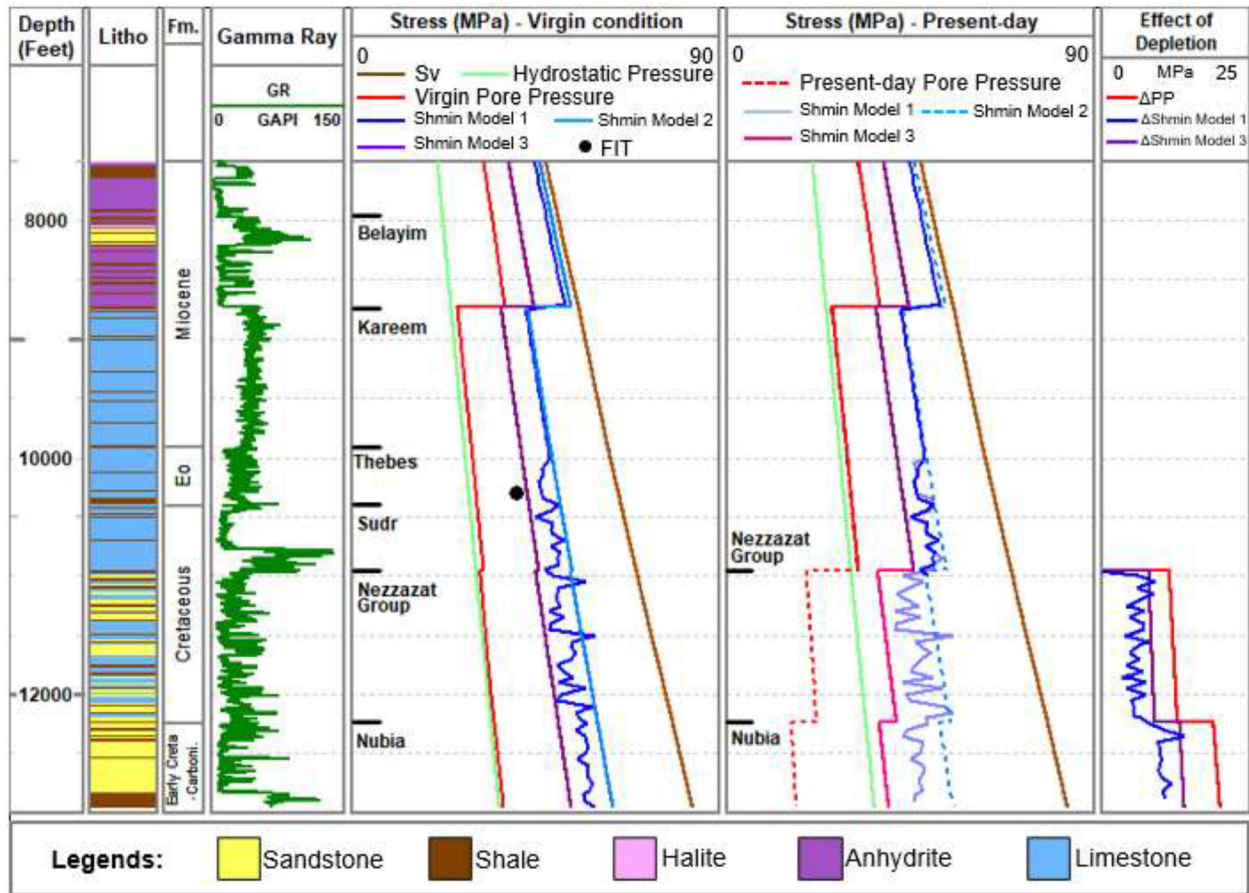
Figure 4. PP and Shmin profiles of the Well B2 in virgin vs depleted conditions. PP and Shin are reduced in the Nezzazat and Nubia reservoirs due to depletion. The rightmost track quantifies the drop in PP and Shmin (ΔPP and ΔShmin, respectively) across the producing reservoirs.

were interpreted to have a 10.7 MPa/km (0.47 PSI/ft) gradient. The Shmin was modeled using three approaches (Fig. 3).

The uniaxial strain model (Shmin-Model 1) and effective stress ratio-based method (Shmin-Model 2) provided a close Shmin gradient range of 15.57–16.47 MPa/km (0.69–0.73 PSI/ft) against the Nezzazat and Nubia reservoir intervals (Fig. 3). The Shmin-Model 2 can be considered to be the higher estimate of the Shmin, as seen from the results, although the dynamic Poisson's ratio-based Shmin-Model 1 depicts the lithological variability in the Shmin estimation in a better way. Due to the unavailability of any leak-off test or mini-frac data, these two Shmin estimates could not be accurately validated. Therefore, we employed the frictional faulting theory and provided Shmin-Model 3, which infers a Shmin lower limit with a gradient of about 14.31 MPa/km (0.63 PSI/ft) in the Lower Creta-

ceous–Carboniferous reservoirs. The available formation integrity test (FIT) measurements were found to be in good accordance with the interpreted Shmin lower limit model (Shmin-Model 3 > FIT) (Fig. 3). Being in a normal faulting tectonic setup, the maximum horizontal stress magnitude can be safely assumed between the Shmin higher estimate (Shmin-Model 2) and Sv. Figure 3 presents the interpreted pore pressure and stresses of the virgin reservoirs in the October oil field.

Effect of Depletion on PP and Shmin

Reservoir pressure measurements throughout the production span were used to interpret the drop in reservoir pore pressure as an effect of continued depletion. The latest measurements indicated a pressure drop of around 11.7–12.7 MPa (1697–1842

PSI) in the Nezzazat Group reservoirs, while the Nubia sandstones were more depleted in the range of 19–21 MPa (2756–3046 PSI) (Fig. 4). It is to be noted that Nubia reservoir was brought to production before the Nezzazat reservoir intervals and it was subjected to a longer production duration, which is reflected by the higher magnitude of depletion. Based on the quantified ΔPP and log-derived Poisson's ratio, we estimated the Shmin profiles against the depleted intervals. Results indicate ΔShmin-Model 1 of 5.5–7.5 MPa (797–1088 PSI) in the Nezzazat Group and 9.5–11.8 MPa (1378–1711 PSI) in the Nubia Formation (Fig. 4). The Shmin

lower limit also responded similarly. The ΔShmin-Model 3 of about 8–9 MPa (1160–1305 PSI) and 13.3–14 MPa (1929–2030 PSI) were recorded against the upper and lower reservoir intervals, respectively.

Implications on Reservoir Stability

Based on the ΔPP and ΔShmin-Model 1, poroelasticity-based stress path values were generated in the producing reservoirs. The Nezzazat and Nubia reservoirs exhibited stress path values of about 0.61 and 0.65, respectively (Fig. 5). Now, considering the
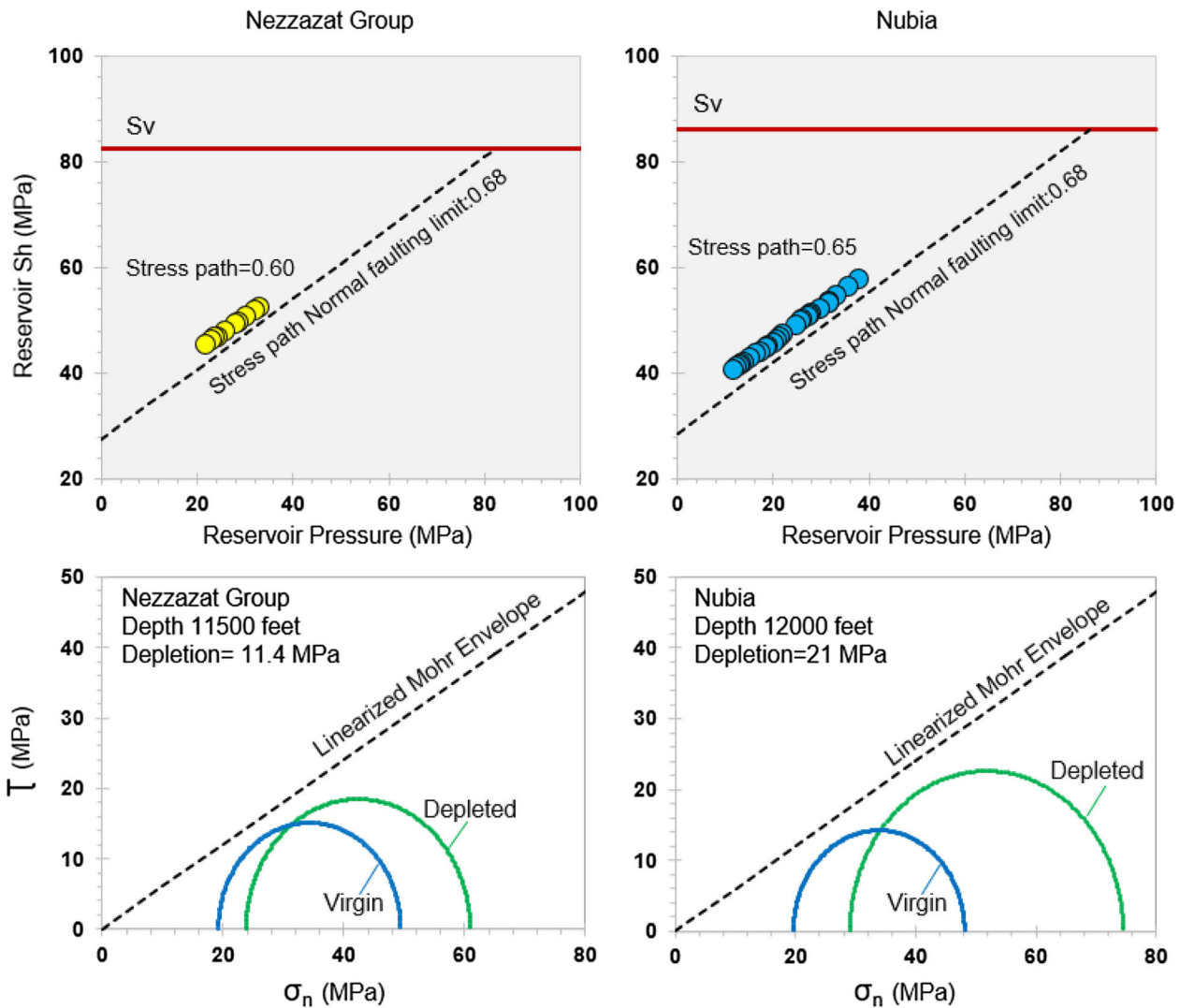
Figure 5. Depletion stress paths of the Nezzazat and Nubia reservoirs of the October oil field based on the PP–Shmin coupling approach. The Nubia reservoir shows a higher stress path value, closer to the normal faulting limit (0.68). For Sv, we utilized the Shmin-Model 1 in this plot. Mohr circles of the virgin and depleted conditions are plotted for both reservoirs at the mentioned depth intervals and depletion magnitudes.

normal faulting stress path limit value of 0.68, production-induced normal faulting is unlikely in both the reservoirs; however, the Nubia reservoir interval is very close to the critical faulting limit/unstable stress path and a continued drawdown with a higher depletion rate might result into an unstable stress path. The depletion stress path values of the upper and lower reservoir intervals were very similar to the Southern North Sea sandstone producer (Fang and Khaskar 2010) and Wytch Farm, UK (Addis 1997).

Implications on Drilling

The earliest downhole measurements indicated about 8.7 PPG (pore pressure gradient) (mud weight equivalent) in the studied reservoirs at virgin conditions. Due to prolonged production, the latest PPG in the depleted Nezzazat and Nubia was inferred as 5.5 and 4 PPG, respectively (Fig. 6). This has critical implications in the drilling design of the future infill injector wells. In the initial field development stage, the drilling mud window between 9 and 12.5 PPG was followed based on the virgin pore pressure and FIT bounds. This window was prevalent from the top of Kareem Formation (or the base of anhydrite of Belayim Formation) to the well TD (target depth) covering both the clastic reservoirs, which allowed drilling the entire mentioned section with a single casing. However, the present depletion profile demands a major revision in the downhole safe mud window.

At the present-day condition, the conservative Shmin lower limit (by Model 3) suggested a value of 9.3 PPG (Fig. 6), which should be considered the highest allowable mud weight in the reservoir sections while drilling future wells. It is to be noted that this upper limit of 9.3 PPG was much lower than the earlier FIT values (12.5 PPG) and indeed very close to the lower mud weight limit, which used to be followed in early field development stages (Fig. 6). At present day, the lower mud weight limit was inferred as 5.5 PPG, as seen from the depleted Nezzazat pore pressure gradient. Overall, a new mud window of 5.5–9.3 PPG was suggested in the depleted section (Fig. 6). This also demands a revised casing design. Revised mud window indicated that the Nezzazat and Nubia sandstone reservoirs should be drilled as a new separate section and to be cased accordingly. This suggestion was made based on the most conservative estimate of Shmin (Model 3, as a

lower limit). However, if Shmin-Model 1 is followed as the best case estimate of the Shmin, it would offer a greater mud window limit against the depleted reservoir and it will also negate the necessity of the new casing if the entire section (Kareem Formation to well TD) is drilled within 9–10.7 PPG mud window.

Effect of Fluid Injection: Limit for Reservoir Failure

We analyzed the effect of fluid injection and re-pressurization in both the depleted reservoir intervals to understand the critical pore pressure limit that can introduce the shear slippage on randomly oriented faults or weak planes at the reservoir levels. For failure limit, a linearized Mohr envelope considered the internal friction coefficient value of 0.6. A conservative approach was undertaken assuming zero cohesion on the fault planes. The results are presented in Figure 7. The analysis revealed that a pore pressure increment in the range of 6 MPa (870 PSI) can shift the Mohr circle to the failure line at the Nezzazat Group reservoir level at the present condition. The same for the Nubia sandstone reservoir was around 7.27 MPa (1054 PSI). However, this traditional approach assumes that the total stress distribution is unaffected due to the fluid injection and thus may under-estimate the critical pore pressure limit for fault slippage. Therefore, we investigated possible pore pressure–stress coupling scenarios to infer the maximum pressure limit applicable for the studied reservoirs at their latest depletion stage and compared the outputs with the results from traditional fault slip analysis. The maximum allowable ΔPP before fault reactivation was investigated for various geomechanical conditions, assuming zero cohesion on the pre-existing faults and fractures: (a) traditional approach ($\beta_v = \beta_h = 0$); (b) both Sv and Shmin changes with a similar ratio of 0.5 ($\beta_v = \beta_h = 0.5$) in response to fluid injection; (c) Shmin coupling with ΔPP during the injection[1]; and (d) both Sv and Shmin are affected by ΔPP during the injection.[2]

Results are presented in Figures 8 and 9 for the Nezzazat and Nubia reservoirs, respectively. At a

---

[1] Considering $\alpha = 1$ and $\upsilon = 0.25$, Eq. 11 provides $\beta_h = 0.66$, while Sv remain unaffected ($\Delta Sv = 0$) and $\beta_v = 0$. This is a simplified poro-elastic solution.

[2] With the same Biot's and Poisson's ratio values, Eqs. 11–12 results in $\beta h = 0.66$ and $\beta v = 0.33$.
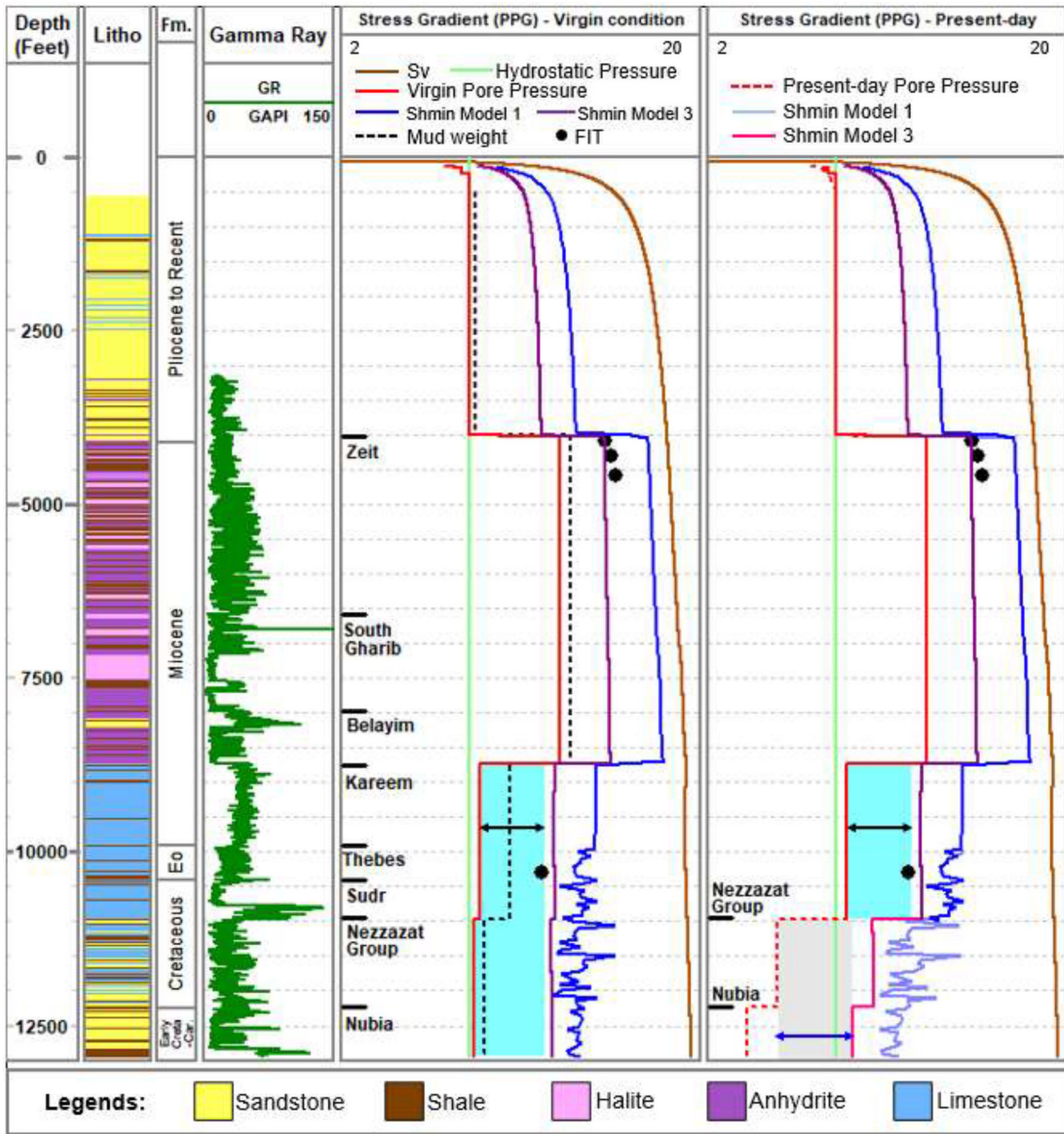
Figure 6. Sv, PP and Shmin gradients (in PPG unit) of the Well B2 in virgin vs depleted conditions. A revised drilling mud window is marked by grey shading (rightmost track) in the depleted Nezzazat and Nubia reservoirs.

depth of 11,500 feet (3505.2 m), the traditional approach provided a maximum ΔPP of 6 MPa (Figs. 7, 8: Case 1), while the critical pressure limit increased in Case 2 with a maximum ΔPP of 8.25 MPa. The stress path slopes were similar in both these situations. In the PP–Shmin coupling situation, Case 3 the injection limit further increased to ΔPP of 23 MPa based on the extensively used poro-elastic approach. In the fourth case, with both the Sv and

Shmin coupling with injection induced pore pressure rise in normal faulting condition, the Mohr circle further shifted to the left and provided the highest ΔPP value. This particular situation is more suitable for the initial pore pressure build-up at the top of the reservoir, i.e., reservoir-seal boundary condition and it does not reflect the stress perturbations within the reservoir, considering a greater vertical thickness of the target injection destination. The
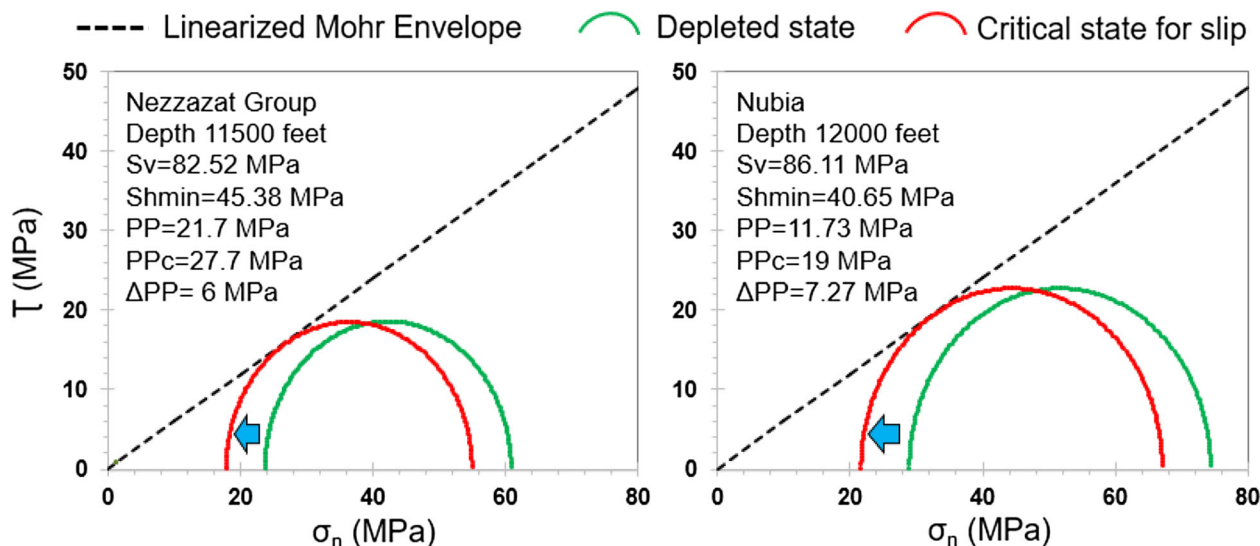
Figure 7. Shear slip criterion along a randomly oriented pre-existing fault or fracture plane due to critical pore fluid pressure. This traditional approach assumes that total stress distribution remains unchanged during the injection. 'σ_n' = effective normal stress along the x-axis. 'τ' = shear stress along the y-axis. A linearized Mohr envelope is presented assuming zero cohesion and $\mu = 0.6$.

same models for Nubia sandstone reservoir at around 12,000 feet (3657.6 m) are presented in Figure 9. Considering PP–Shmin coupling, Nubia sandstone reservoir provided an injection pressure build-up tolerance of approximately 27 MPa, which is three times of the traditional approach-based estimation.

Effect of Fluid Injection on Caprock Integrity

To infer the geomechanical stability of the caprock, it was assessed by Eq. 15. We assumed the tensile strength of the caprock to be negligible. In absence of definite leak-off pressure measurement, the Shmin of the overlying rock was considered as FP_{Cap} (Eq. 15). In addition, the lower limit of Shmin (Model 3) was used to characterize this integrity aspect from a more conservative approach. For the Nezzazat Group of reservoirs, the Upper Cretaceous Sudr–Brown Limestones act as the sealing rock, which yielded a gradient of about 14 MPa/km against the Shmin-Model 3 (Fig. 4), which translates to 48 MPa Shmin magnitude at the base of the caprock (top of Nezzazat). The maximum allowable ΔPP models for injection in the Nezzazat reservoirs (Fig. 8) indicated that in Case 1–3 injections (PP + ΔPP) < FP_{Cap}., and caprock stability will not be affected. However, the total pressure build-up in the Case 4 injection model (Fig. 8) is likely to exceed

the Shmin lower estimate of the caprock carbonates and can induce hydraulic fracturing.

The same analysis was run for the Nubia sandstone reservoir; this became more complicated as the depleted Nezzazat Group acts as the caprock. These two reservoirs are separated by thin dolomite and shale intervals of the Lower Raha Formation. At the present depleted stage, Shmin-Model 3 had a magnitude of 42 MPa at 12,225 feet (3726.2 m) (base of Raha and top of Nubia). When compared with the injection maximum allowable ΔPP models in Nubia sandstone reservoir (Fig. 9), Case 1–3 satisfied the caprock stability criterion, but Case 4 had the likelihood to fail the Raha caprock above Nubia Formation. Therefore, the maximum injection limit in both the reservoirs must be guided by the caprock integrity threshold. The fluid injection in the depleted Nubia sandstone reservoir started in 1996 and the pore pressure build-up measurements were available during the interval 1996–2000. At 12,000 feet (3657.6 m) level, reservoir pore pressure increased to 17.25 MPa after 4 years of the injection process, while the lowest PP of pre-injection level (during 1996) was recorded as 11.73 MPa. The reported injection-induced pressure build-up ($\sim$ 5.52 MPa in 4 years) was well below the critical pressure estimates of Case 1 (traditional approach) and Case 3 (PP–Shmin coupling situation) as well as the conservative Shmin estimate of the Nezzazat caprock; thus, negating reservoir failure chances and maintaining caprock stability.
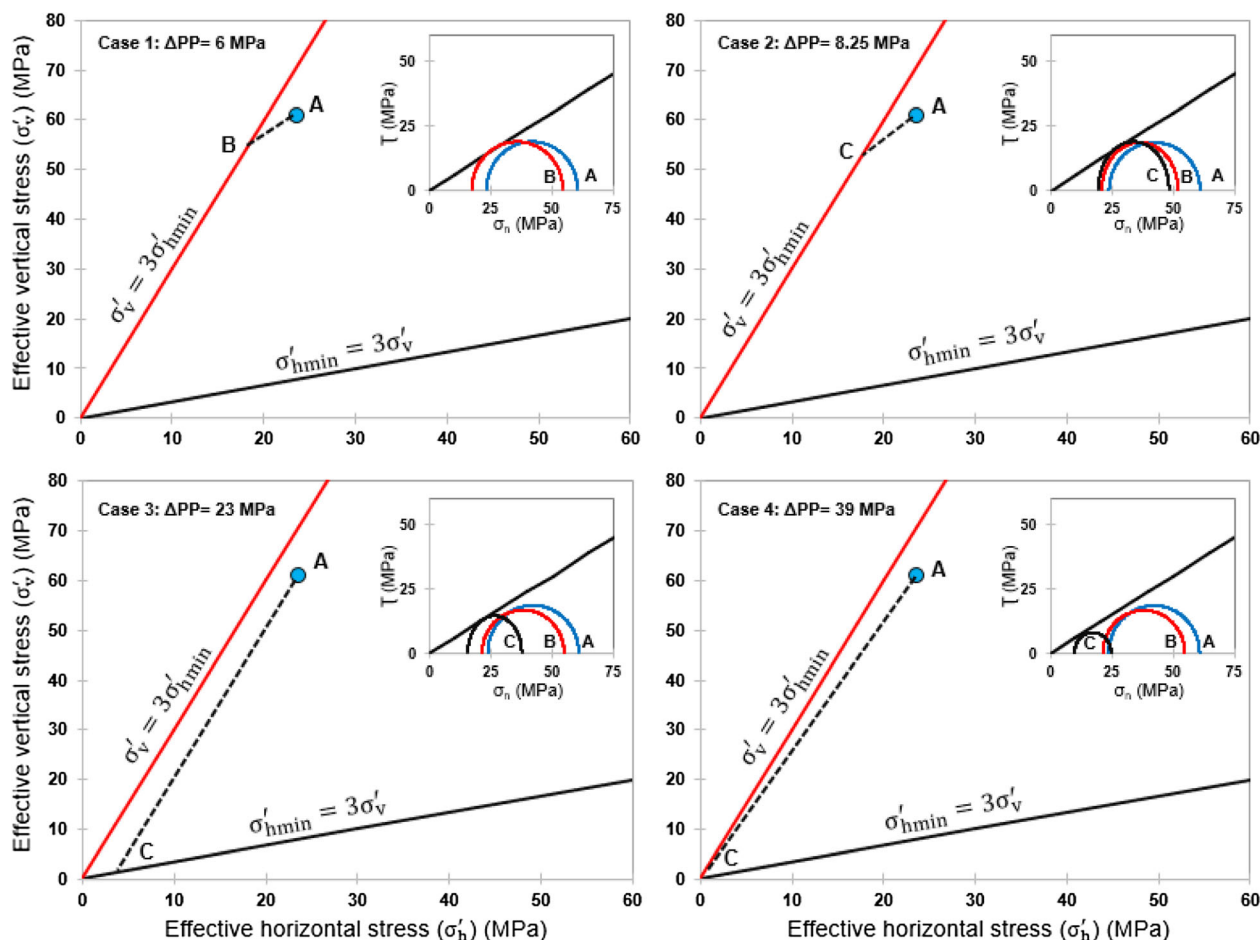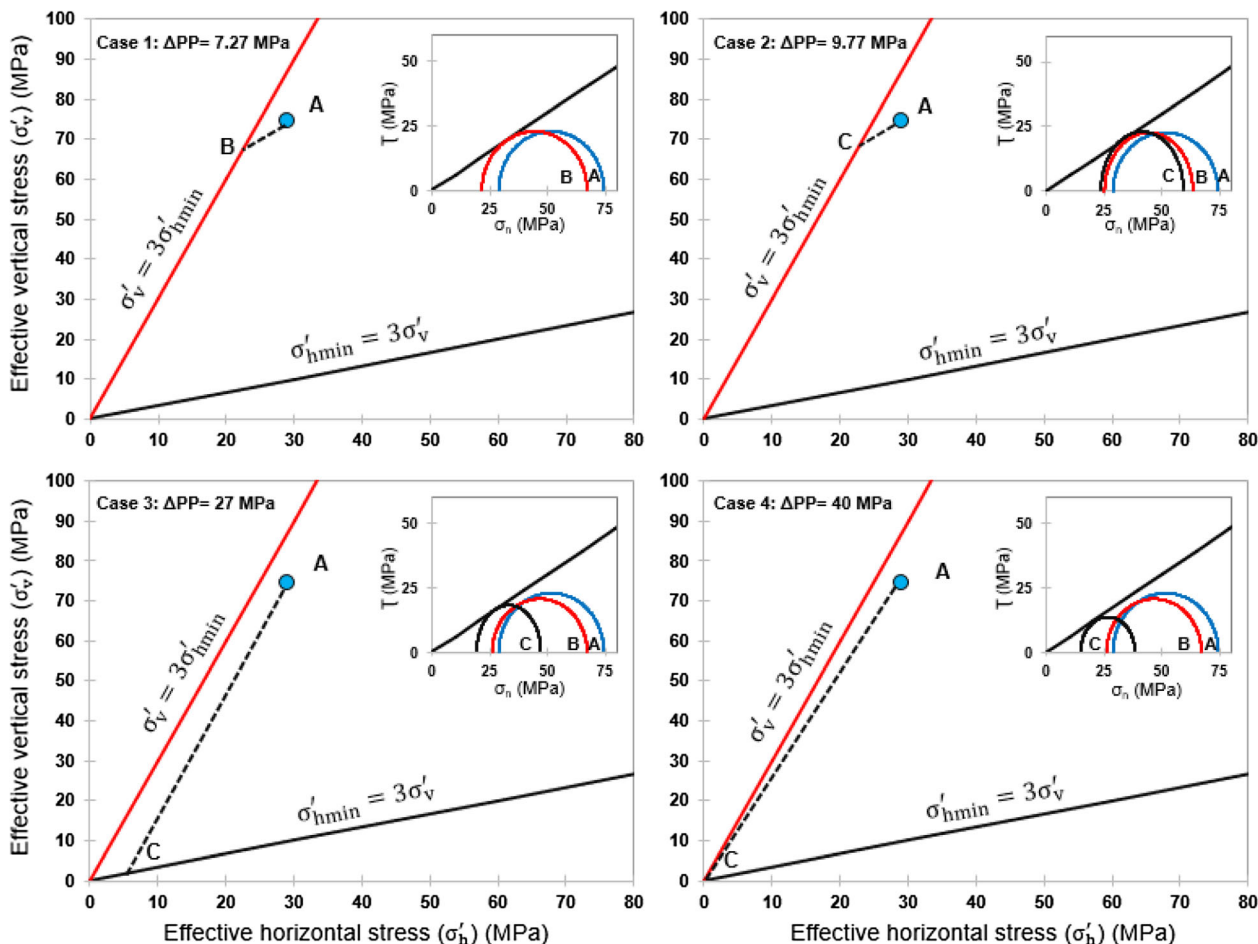
Figure 8. Injection stress path models and the maximum allowable pore pressure change (ΔPP) of the Nezzazat reservoir in four different conditions: **a** Case 1: traditional approach, $\beta_v = \beta_h = 0$; **b** Case 2: $\beta_v = \beta_h = 0.5$; **c** Case 3: $\beta_h = 0.66$ and $\Delta Sv = 0$; and **d** Case 4: $\beta_h = 0.66$ and $\beta_v = 0.33$. Corresponding Mohr Circles are presented in the inset for each case. A = Mohr circle at the latest depletion stage. B = Mohr circle with ΔPP = 6 MPa assuming total stresses unaffected. C = Mohr circle with the required ΔPP to induce fault slip assuming pore pressure-stress coupling during fluid injection.

CONCLUSIONS

This study interpreted the PP, Sv and Shmin magnitudes in the October oil field to infer the stress paths in depletion as well as fluid injection scenarios. The effect of production-induced depletion was reflected in the PP and Shmin profiles of the Nezzazat and Nubia reservoir intervals. Due to prolonged hydrocarbon production, the present PPG in the Nezzazat and Nubia reservoirs were reduced to 5.5 and 4 PPG, respectively, from an initial 8.7 PPG level. Based on the revised downhole drilling mud window of 5.5–9.3 PPG, optimum mud and casing designs were suggested for future infill/injector drilling campaign to ensure wellbore safety and integrity. The depletion stress path was deduced from

PP–Shmin coupling to comment on the reservoir stability in response to production. Mean stress path values for both the reservoirs were away from the critical normal faulting limit at the present rate of depletion. However, the Nubia reservoir interval was very close to the critical faulting limit/unstable stress path and a continued drawdown with a higher depletion rate might result in an unstable stress path. Water flooding is being actively engaged in the October oil field to maintain the production performance. This study analyzed four different geomechanical scenarios to understand the fault reactivation potential of the depleted reservoirs due to fluid injection. Considering that the maximum injection threshold should be guided by the caprock integrity, this study provided the critical

Figure 9. Injection stress path models and the maximum allowable pore pressure change (ΔPP) of the Nubia reservoir in four different conditions: **a** Case 1: traditional approach, $\beta_v = \beta_h = 0$; **b** Case 2: $\beta_v = \beta_h = 0.5$; **c** Case 3: $\beta_h = 0.66$ and $\Delta Sv = 0$; and **d** Case 4: $\beta_h = 0.66$ and $\beta_v = 0.33$. Corresponding Mohr Circles are presented in the inset for each case. A = Mohr circle at the latest depletion stage. B = Mohr circle with $\Delta PP = 7.27$ MPa assuming total stresses unaffected. C = Mohr circle with the required ΔPP to induce fault slip assuming pore pressure-stress coupling during fluid injection.

injection-induced pore pressure build-up limit for both the reservoirs utilizing the pore pressure in situ stress coupling approach.

REFERENCES

Abdelghany, W. K., Radwan, A. E., Elkhawaga, M. A., Wood, D. A., Sen, S., & Kassem, A. A. (2021). Geomechanical modeling using the depth-of-damage approach to achieve successful underbalanced drilling in the gulf of suez rift basin. *Journal of Petroleum Science and Engineering.* https://doi.org/10.1016/j.petrol.2020.108311.

Abudeif, A. M., Attia, M. M., & Radwan, A. E. (2016a). Petro-physical and petrographic evaluation of Sidri Member of Belayim Formation, Badri field, Gulf of Suez Egypt. *Journal of African Earth Sciences, 115,* 108–120.

Abudeif, A. M., Attia, M. M., & Radwan, A. E. (2016b). New simulation technique to estimate the hydrocarbon type for the two untested members of Belayim Formation in the absence of pressure data, Badri Field, Gulf of Suez Egypt. *Arabian Journal of Geosciences, 9*(3), 218. https://doi.org/10.1007/s12517-015-2082-2.

Abudeif, A. M., Attia, M. M., Al-Khashab, H. M., & Radwan, A. E. (2018). Hydrocarbon type detection using the synthetic logs: A case study, Baba member, Gulf of Suez Egypt. *Journal of African Earth Sciences, 144,* 176–182.

Addis, M. A. (1997). Reservoir depletion and its effect on well-bore stability evaluation. *International Journal of Rock Mechanics and Mining Sciences, 34*(3–4), 4.e1–4.e17. https://doi.org/10.1016/S1365-1609(97)00238-4.

Addis, M. A., Last, N. C., & Yassir, N. A. (1994). The estimation of horizontal stresses at depth in faulted regions and their relationship to pore pressure variations. In *Rock Mechanics in Petroleum Engineering Conference, Delft, Netherlands, August 29–31.* https://doi.org/10.2118/28140-MS.

Agbasi, O. E., Sen, S., Inyang, N. J., & Etuk, S. E. (2021). Assessment of pore pressure, wellbore failure and reservoir stability in the Gabo field, Niger Delta, Nigeria: Implications for drilling and reservoir management. *Journal of African Earth Sciences, 173,* 104038.

Alsharhan, A. S. (2003). Petroleum geology and potential hydrocarbon plays in the Gulf of Suez rift basin Egypt. *AAPG Bulletin, 87*(1), 143–180.

Alsharhan, A. S., & Salah, M. G. (1995). Geology and hydrocarbon habitat in rift setting: northern and central Gulf of Suez Egypt. *Bulletin of Canadian Petroleum Geology, 43*(2), 156–176.

Altmann, J. B., Muller, T. M., Muller, B. I. R., Tingay, M. R. P., & Heidbach, O. (2010). Poroelastic contribution to the reservoir stress path. *International Journal of Rock Mechanics and Mining Sciences, 47*(7), 1104–1113.

Askar, M., Abdallah, A., & Gad, I. (2020). Downhole scales associated with October Field formation waters and water injection using a shallow aquifer. In *SPE International conference and exhibition on formation damage control, Lafayette, Louisiana, USA, Feb 19–21.* SPE-199300-MS. https://doi.org/10.2118/199300-MS.

Attia, I., Helal, I., El Dakhakhny, A., & Aly, S. A. (2017). Using sequence stratigraphic approaches in a highly tectonic area: Case study–Nubia (A) sandstone in southwestern Gulf of Suez Egypt. *Journal of African Earth Sciences, 136,* 10–21.

Attia, M. M., Abudeif, A. M., & Radwan, A. E. (2015). Petro-physical analysis and hydrocarbon potentialities of the untested Middle Miocene Sidri and Baba sandstone of Belayim Formation, Badri field, Gulf of Suez Egypt. *Journal of African Earth Sciences, 109,* 120–130.

Bale, A., Fossen, H., Berg, E., Mjelde, O., & Kui, T. (2008). Comprehensive mini-frac testing in the gullfaks field as a tool for characterization of reservoir structure and rock mechanics. In *International petroleum technology conference held in Kuala Lumpur, Malaysia, Dec 3–5.* IPTC-11968-MS.

Baouche, R., Sen, S., & Boutaleb, K. (2020a). Present day In-situ stress magnitude and orientation of horizontal stress components in the eastern Illizi basin, Algeria: A geomechanical modeling. *Journal of Structural Geology, 132,* 103975.

Baouche, R., Sen, S., & Boutaleb, K. (2020b). Distribution of pore pressure and fracture pressure gradients in the Paleozoic sediments of Takouazet field, Illizi basin Algeria. *Journal of African Earth Sciences, 164*, 103778. https://doi.org/10.1016/j.jafrearsci.2020.103778.

Baouche, R., Sen, S., Sadaoui, M., Boutaleb, K., & Ganguli, S. S. (2020c). Characterization of pore pressure, fracture pressure, shear failure and its implications for drilling, wellbore stability and completion design: A case study from the Takouazet field, Illizi Basin Algeria. *Marine and Petroleum Geology, 120,* 104510.

Baouche, R., Sen, S., & Ganguli, S. S. (2020d). Pore pressure and in-situ stress magnitudes in the Bhiret Hammou hydrocarbon field, Berkine Basin Algeria. *Journal of African Earth Sciences, 171,* 103945.

Borling, D. C., Powers, B. S., & Ramadan, N. (1996). Water shut-off case history using Through-Tubing Bridge Plugs; October field, Nubia Formation, Gulf of Suez, Egypt. In *Abu Dhabi International Petroleum Exhibition and Conference, Abu Dhabi, United Arab Emirates, Oct 13–16. SPE-36213.* https://doi.org/10.2118/36213-MS.

Bosworth, W., & McClay, K. (2001). Structural and stratigraphic evolution of the Gulf of Suez rift, Egypt: A synthesis. Mémoires du Muséum national d'histoire naturelle, Vol. 186, pp. 567–606.

Chan, A. W., & Zoback, M. D. (2002). Deformation analysis in reservoir space (DARS): A simple formalism for prediction of reservoir deformation with depletion. In *SPE/ISRM Rock mechanics conference, Irving, Texas, Oct 20–23.* SPE/ISRM 78174.

Chiaramonte, L., Zoback, M. D., Friedmann, J., & Stamp, V. (2008). Seal integrity and feasibility of CO_2 sequestration in the Teapot Dome EOR pilot: Geomechanical site characterization. *Environmental Geology, 54,* 1667–1675.

Chowdhary, L. R., & Taha, S. (1987). Geology and habitat of oil in Ras Budran field, G.O.S Egypt. *AAPG Bulletin, 71*(10), 1274–1293.

Dolson, J. (2020). The petroleum geology of Egypt and history of exploration. In *The Geology of Egypt*, Springer, Cham (pp. 635–658).

Egyptian General Petroleum Corporation (EGPC), (1996). Gulf of Suez oil fields (A comprehensive overview).

El-Gendy, N., Barakat, M., & Abdallah, H. (2017). Reservoir assessment of the Nubian sandstone reservoir in South Central Gulf of Suez Egypt. *Journal of African Earth Sciences, 129,* 596–609.

El-Ghamri, M. A., Warburton, I. C., & Burley, S. D. (2002). Hydrocarbon generation and charging in the October Field Gulf of Suez, Egypt. *Journal of Petroleum Geology, 25*(4), 433–464.

El Nady, M. M. (2006). The hydrocarbon potential of Miocene source rocks for oil generation in the South Gulf of Suez Egypt. *Petroleum Science and Technology, 24*(5), 539–562.

El Nady, M. M., Barakat, A. M., & Harb, F. M. (2007). Crude oil geochemistry and timing of petroleum generation in the Central Gulf of Suez Egypt. *Journal Egyptian Petroleum, 16*(2), 137–155.

El Sharawy, M. S., & Nabawy, B. S. (2016). Geological and petrophysical characterization of the lower Senonian Matulla formation in southern and central Gulf of Suez Egypt. *Arabian Journal for Science and Engineering, 41*(1), 281–300.

Fang, Z., & Khaskar, A. (2010). Geomechanical assessment for underground gas storage and CO2 sequestration in depleted hydrocarbon reservoirs. In *SPE Asia pacific oil and gas conference and exhibition, Brisbane, Australia, Oct 18–20.* SPE-133994-MS. https://doi.org/10.2118/133994-MS.

Fang, Z., & Khaskar, A. (2013). Role of geomechanics in assessing the feasibility of CO_2 sequestration in depleted hydrocarbon sandstone reservoirs. *Rock Mechanics and Rock Engineering, 46*(3), 479–497.

Figueiredo, B., Tsang, C.-F., Rutqvist, J., Bensabat, J., & Niemi, A. (2015). Coupled hydro-mechanical processes and fault reactivation induced by CO_2 Injection in a three-layer stor-

age formation. *International Journal of Greenhouse Gas Control, 39,* 432–448.

Fjær, E., Holt, R. M., Raaen, A., Risnes, R., & Horsrud, P. (2008). Petroleum related rock mechanics (2nd edition), *Developments in Petroleum Science, 53*. Amsterdam, Elsevier.

Ganguli, S. S., Dimri, V. P., & Sen, S., (2018). A Comprehensive Geomechanical Assessment of an Indian Mature Oil Field for CO$_2$-Enhanced Oil Recovery and its Sequestration. In *American Geophysical Union (AGU) Fall Meeting, Washington, DC, Dec 10–14.*.

Ganguli, S. S., & Sen, S. (2020). Investigation of present-day in-situ stresses and pore pressure in the south Cambay Basin, western India: Implications for drilling, reservoir development and fault reactivation. *Marine and Petroleum Geology, 118,* 104422.

Goulty, N. R. (2003). Reservoir stress path during depletion of Norwegian chalk oilfields. *Petroleum Geoscience, 9*(3), 233–241.

Geertsma, J. (1957). The effect of fluid pressure decline on volumetric changes of porous rocks. *Transactions of the AIME*, *210*(01), 331–340. https://doi.org/10.2118/728-G.

Geertsma, J. (1966). Problems of rock mechanics in petroleum production engineering. In *1st ISRM Congress, Lisbon, Portugal, Sept 25–Oct 1*. ISRM-1CONGRESS-1966-099.

Hassan, N. R., Rocha, G., Michel, C. M., & Hey, M.-J. V. (2006). Donwhole integrity management in October field, Gulf of Suez, Egypt. In *SPE Abu Dhabi International Petroleum Exhibition and Conference, Abu Dhabi, UAE, Nov 5–8*. SPE-100600. https://doi.org/10.2118/100600-MS.

Haug, C., Nüchter, J.-A., & Henk, A. (2018). Assessment of geological factors potentially affecting production-induced seismicity in North German gas field. *Geomechanics for Energy and Environment, 16,* 15–31.

Hawkes, C. D., McLellan, P. J., & Bachu, S. (2004). Geomechanical factors affecting geological storage of CO$_2$ in depleted oil and gas reservoirs: Risks and mechanisms. In *6th North America Rock Mechanics Symposium (NARMS), Houston, Texas, June 5–9*. ARMA-04-579.

Hillis, R. (2000). Pore pressure/stress coupling and its implications for seismicity. *Exploration Geophysics, 31*(2), 448–454.

Ibrahim, A. A., & Mostafa, A. (1999). Production logging problem description in October field, Gulf of Suez. In *SPE Annual Technical Conference and Exhibition, Houston, Texas, Oct 3–6*. SPE 56650.

Ibrahim, M. M., Styler, J. W., Shamma, H. L., Elsherif, M. A., & AboElalla, E. M. (2008). Environmentally friendly and economic waterflood system for October Field at Gulf of Suez, Egypt. In *Indian Oil and Gas Technical Conference and Exhibition, Mumbai, India, Mar 4–6*. SPE-112311-MS. https://doi.org/10.2118/112311-MS.

Jaeger, J. C., Cook, N. G. W., & Zimmerman, R. (2007). *Fundamentals of rock mechanics* (4th ed.). Oxford: Wiley-Blackwell.

Kassem, A. (2018). Diagenetic history and its effect on reservoir quality and reservoir characterization of sandstone sequences of Matulla formation, October field, Gulf of Suez, Egypt. In *AAPG International Conference and Exhibition, Cape Town, South Africa, Nov 4–11*. Search and Discovery Article #90332.

Kassem, A., Hemdan, K., Sakr, S., Reda, O., & Saad, A. (2017). Integration of petrology and petrophysical rock typing for optimum reservoir zonation and permeability prediction-case study: north Gulf of Suez, Egypt. In *Offshore Mediterranean Conference and Exhibition, Ravenna, Italy, Mar 29–31*. OMC-2017-524.

Kassem, A., Sharaf, L. M., Baghdady, A. R., & El-Naby, A. E. (2020). Cenomanian/Turonian oceanic anoxic event 2 in October oil field, central Gulf of Suez Egypt. *African Journal of Earth Sciences, 165,* 103817.

Kassem, A. A., Hussein, W., Radwan, A. E., Nasr, A., Abioui, M., Jain, S., et al. (2021). Petrographic and diagenetic study of siliciclastic jurassic sediments from the northeastern margin of Africa: Implication for reservoir quality. *Journal of Petroleum Science and Engineering*, *200*, 108340.

Kenter, C. J., Blanton, T. L., Schreppers, G. M. A., Baaijens, M. N., & Ramos, G. G. (1998). Compaction Study for Shearwater Field. In *SPE/ISRM Rock Mechanics in Petroleum Engineering, Trondheim, Norway, July 8–10*. SPE-47280-MS.

Khaksar, A., Taylor, P. G., Fang, Z., Kayes, T., Salazar, A., & Rahman, K. (2009). Rock Strength from Core and Logs: Where We Stand and Ways to Go. In *SPE EUROPEC/ EAGE Annual Conference and Exhibition held in Amsterdam, The Netherlands, June 8–11*, SPE 121972.

Kim, S., & Hosseini, S. A. (2014). Geological CO$_2$ storage: incorporation of pore-pressure/stress coupling and thermal effects to determine maximum sustainable pressure limit. *Energy Procedia, 63,* 3339–3346.

Kim, S., & Hosseini, S. A. (2016). Study on the ratio of pore-pressure/stress changes during fluid injection and its implications for CO2 geologic storage. *Journal of Petroleum Science and Engineering, 149,* 138–150.

Lelek, J. J., Shepherd, D. B., Stone, D. M., & Abdine, A. S. (1992). October Field - the latest giant under development in Egypt's Gulf of Suez. In M. T. Halbouty (Ed.), Giant Oil and Gas Fields of the Decade 1978–1988. *AAPG Memoir, 54*, 231–249. https://doi.org/10.1306/M54555.

Liu, S., & Harpalani, S. (2014). Evaluation of in situ stress changes with gas depletion of coalbed methane reservoirs. *Journal of Geophysical Research Solid Earth, 119,* 6263–6276.

Lorenz, J. C., Teufel, L. W., & Warpinski, R. (1991). Regional fractures I: A mechanism for the formation of regional fractures at depth in flat-lying reservoirs. *AAPG Bulletin, 75,* 1714–1737.

Lyberis, N. (1988). Tectonic evolution of the Gulf of Suez and the Gulf of Aqaba. *Tectonophysics, 153*(1–4), 209–220.

Lynch, T., Fisher, Q., Angus, D., & Lorinczi, P. (2013). Investigating stress path hysteresis in a CO$_2$ injection scenario using coupled geomechanical-fluid flow modelling. *Energy Procedia, 37,* 3833–3841.

Matthews, W. R., & Kelly, J. (1967). How to predict formation pressure and fracture gradient. *Oil and Gas Journal, 65*(8), 92–106.

Morris, J. P., Hao, Y., Foxall, W., & McNab, W. (2010). A study of injection induced mechanical deformation at the In Salah CO$_2$ storage project. In *44th U.S. rock mechanics symposium and 5th U.S.–Canada rock mechanics symposium, Salt Lake City, Utah, June 27–30*. ARMA10-307.

Mulders, F. M. M. (2003). Modelling of stress development and fault slip in and around a producing gas reservoir. *Ph.D. Thesis. Delft University of Technology, Netherlands*.

Nabawy, B. S., & El Sharawy, M. S. (2018). Reservoir assessment and quality discrimination of Kareem Formation using integrated petrophysical data, Southern Gulf of Suez Egypt. *Marine and Petroleum Geology, 93,* 230–246.

Nassar, I. S., Noureldien, D. M. (2013). A case study from October Field: Modeling heterogeneity results in improved reservoir management. In *SPE Reservoir Characterization and Simulation Conference and Exhibition. Abu Dhabi, UAE, Sep 16–18*. SPE 165939. https://doi.org/10.2118/165939-MS.

Nelson, E. J., Hillis, R. R., Meyer, J J., Mildren, S. D., Nispen, D. V., & Briner, A. (2005). The reservoir stress path and its implications for water-flooding, Champion Southeast field, Brunei. In *40th U.S. Symposium on Rock Mechanics (USRMS), Anchorage, Alaska, June 25–29*. ARMA-05-775.

Noureldien, D. M., & Nabil, S. (2016). GUPCO experience with giant fields: Case studied from Egypt. In *Abu Dhabi International Petroleum Exhibition and Conference, Abu Dhabi,*

UAE, Nov 7–10. SPE-183556-MS. https://doi.org/10.2118/183556-MS.

Olson, J. E., Laubach, S. E., & Lander, R. H. (2009). Natural fracture characterization in tight gas sandstones: Integrating mechanics and diagenesis. *AAPG Bulletin, 93*(11), 1535–1549.

Plumb, R. A., Evans, K. F., & Engelder, T. (1991). Geophysical log responses and their correlation with bed to bed stress contrasts in Paleozoic rocks, Appalachian plateau, New York. *Journal of Geophysical Research, 96*(B9), 4509–14528.

Radwan, A., & Sen, S. (2021). Stress path analysis for characterization of in situ stress state and effect of reservoir depletion on present-day stress magnitudes: Reservoir geomechanical modeling in the Gulf of Suez Rift Basin Egypt. *Natural Resources Research, 30,* 463–478. https://doi.org/10.1007/s11053-020-09731-2.

Radwan, A. E. (2021). Modeling the depositional environment of the sandstone reservoir in the middle miocene sidri member, badri field, gulf of suez basin, Egypt: integration of gamma-ray log patterns and petrographic characteristics of lithology. *Natural Resources Research, 30*, 431–449. https://doi.org/10.1007/s11053-020-09757-6.

Radwan, A. E., Abudeif, A. M., Attia, M. M., & Mohammed, M. A. (2019a). Pore and fracture pressure modeling using direct and indirect methods in Badri Field, Gulf of Suez Egypt. *Journal of African Earth Sciences, 156,* 133–143.

Radwan, A. E., Abudeif, A. M., Attia, M. M., & Mahmoud, M. A. (2019b). Development of formation damage diagnosis workflow, application on Hammam Faraun reservoir: A case study, Gulf of Suez Egypt. *Journal of African Earth Sciences, 153,* 42–53.

Radwan, A. E., Abudeif, A., Attia, M., & Mahmoud, M. (2019c). Formation damage diagnosis, application on hammam faraun reservoir: A case study, Gulf of Suez, Egypt. In *Offshore Mediterranean Conference.* https://doi.org/10.13140/RG.2.2.22352.66569.

Radwan, A. E., Abudeif, A., Attia, M., & Mahmoud, M. (2019d). Development of formation damage diagnosis workflow, application on Hammam Faraun reservoir: a case study, Gulf of Suez, Egypt. In *Offshore Mediterranean Conference.* ISBN9788894043679-2019.

Radwan, A. E., Abudeif, A. M., Attia, M. M., Elkhawaga, M. A., Abdelghany, W. K., & Kasem, A. A. (2020a). Geopressure evaluation using integrated basin modelling, well-logging and reservoir data analysis in the northern part of the Badri oil field, Gulf of Suez Egypt. *Journal of African Earth Sciences, 162,* 103743.

Radwan, A. E., Kassem, A. A., & Kassem, A. (2020b). Radwany formation: A new formation name for the Early-Middle Eocene carbonate sediments of the offshore October oil field, Gulf of Suez: Contribution to the Eocene sediments in Egypt. *Marine and Petroleum Geology, 116,* 104304.

Radwan, A. E., Abudeif, A. M., & Attia, M. M. (2020c). Investigative petrophysical fingerprint technique using conventional and synthetic logs in siliciclastic reservoirs: A case study, Gulf of Suez basin Egypt. *Journal of African Earth Sciences, 167,* 103868.

Radwan, A. E., Trippetta, F., Kassem, A. A., & Kania, M. (2021a). Multi-scale characterization of unconventional tight carbonate reservoir: Insights from October oil filed, Gulf of Suez rift basin Egypt. *Journal of Petroleum Science and Engineering, 197*, 107968. https://doi.org/10.1016/j.petrol.2020.107968.

Radwan, A.E., Nabawy, B., Kassem, A. A., & Hussein, W. (2021b). Implementation of rock typing on waterflooding process during secondary recovery in oil reservoirs: A case study, El Morgan Oil Field, Gulf of Suez, Egypt. *Natural Resources Research*. https://doi.org/10.1007/s11053-020-09806-0.

Rutqvist, J., Vasco, D. W., & Myer, L. (2009). Coupled reservoir geomechanical analysis of CO_2 injection at In Salah, Algeria. *Energy Procedia, 1,* 1847–1854.

Safari, M. R., Trevor, O., Queena, C., Hamed, C., Blair, N., Uno, M., & Hawkes, C.D. (2013). Effect of depletion/injection induced stress changes on natural fracture reactivation. In *47th U.S. Rock Mechanics/Geomechanics Symposium, San Francisco, California, June 23–26*. ARMA-2013-395.

Sallam, E. S., Afife, M. M., Fares, M., van Loon, A. T., & Ruban, D. A. (2019). Depositional cycles of the Lower Miocene Rudeis Formation (southwestern offshore margin of the Gulf of Suez, Egypt): Implications for reservoir evaluation. *Marine Geology, 415,* 105964.

Santarelli, F. J., Tronvoll, J. T., Svennekjaer, M., Skeie, H., Henriksen, R., & Bratli, R. K. (1998). Reservoir stress path: The depletion and the rebound. In *SPE/ISRM Eurock, Trondheim, Norway, July 8–10*. SPE/ISRM 47350.

Schoenball, M., Müller, T., Müller, B., & Heidbach, O. (2010). Fluid-induced microseismicity in prestressed rock masses. *Geophysical Journal International, 180*(2), 813–819.

Segall, P., & Fitzgerald, S. D. (1996). A note on induced stress changes in hydrocarbon and geothermal reservoirs. *Tectonophysics, 289,* 117–128.

Segura, J. M., Fisher, Q. J., Crook, A. J. L., Dutko, M., Yu, J., Skachkov, S., et al. (2011). Reservoir stress path characterization and its implications for fluid-flow production simulation. *Petroleum Geoscience, 17*(4), 335–347.

Sen, S., & Ganguli, S. S. (2019). Estimation of pore pressure and fracture gradient in volve field, Norwegian North Sea. In *SPE Oil and Gas India Conference and Exhibition, Mumbai, India, April 9–11*. SPE 194578. https://doi.org/10.2118/194578-MS.

Sen, S., Kundan, A., Kalpande, V., & Kumar, M. (2019). The present-day state of tectonic stress in the offshore Kutch-Saurashtra Basin, India. *Marine and Petroleum Geology, 102,* 751–758.

Sen, S., Kundan, A., & Kumar, M. (2018a). Post-drill analysis of pore pressure and fracture gradient from well logs and drilling events: an integrated case study of a high pressure exploratory well from Panna East, Mumbai Offshore basin, India. In *Pore Pressure and Geomechanics from Exploration to Abandonment, AAPG Geosciences Technology Workshop, Perth, Australia, June 6–7*. https://doi.org/10.1306/42289Sen2018.

Sen, S., Kundan, A., & Kumar, M. (2020). Modeling pore pressure, fracture pressure and collapse pressure gradients in offshore panna, western India: implications for drilling and wellbore stability. *Natural Resources Research, 29,* 2717–2734. https://doi.org/10.1007/s11053-019-09610-5.

Sen, S., Maxwell, C., & Kumar, M. (2018b). Real time pore pressure interpretation from drilling events: A case study from high pressure offshore exploratory well. In *Operations Geoscience Adding Value, The Geological Society, London, November 7–8.*.

Sen, S., Corless, J., Dasgupta, S., Maxwell C., & Kumar, M. (2017). Issues faced while calculating overburden gradient and picking shale zone to predict pore pressure. In *First EAGE Workshop on Pore Pressure Prediction, Mar 19–21, Pau, France,* Paper Mo PP1B 02. https://doi.org/10.3997/2214-4609.201700042.

Schutz, K. I. (1994). Structure and stratigraphy of the Gulf of Suez, Egypt: *Chapter 2: Part I. Type Basin, Gulf of Suez*.

Sercombe, W. J., Thurmon, L., & Morse, J. (2011). Advanced reservoir modeling in poor seismic; October Field, Northern Gulf of Suez, Egypt. In *AAPG International Conference and Exhibition, Milan, Italy, Oct 23–26*. AAPG Search and Discovery Article #40872.

Soltanzadeh, H., & Hawkes, C. D. (2007). Predicting the stress changes induced by fluid production and injection in porous

reservoirs. In *1st Canada-U.S. Rock Mechanics Symposium, Vancouver, Canada, May 27–31*. ARMA-07-200.

Streit, J. E., & Hillis, R. R. (2004). Estimating fault stability and sustainable fluid pressures for underground storage of CO_2 in porous rock. *Energy, 29*(9–10), 1445–1456.

Taghipour, M., Ghafoori, M., Lashkaripour, G. R., Moghaddas, N. H., & Molaghab, A. (2019). Estimation of the current stress field and fault reactivation analysis in the Asmari reservoir, SW Iran. *Petroleum Science, 16,* 513–526.

Terzaghi, K. (1923). Die Berechnung der Durchlässigkeitziffer des Tonesaus dem Verlauf Spannungserscheinungen, Akad. Der Wissenchafeb in Wien, Sitzungsberichte, Mathematisch-naturwissenschafttliche Klasse. Part Iia 142 (3/4), 125–138.

Teufel, L. W., Rhett, D. W., & Farrell, H. E. (1991). Effect of reservoir depletion and pore pressure drawdown on in situ stress and deformation in the Ekofisk Field, North Sea. *International Journal of Rock Mechanics and Mining Sciences & Geomechanics Abstracts, 29*(2), A101. https://doi.org/10.1016/0148-9062(92)92352-d.

Townend, J., & Zoback, M. D. (2000). How faulting keeps the crust strong. *Geology, 28*(5), 399–402.

Vidal-Gilbert, S., Tenthorey, E., Dewhurst, D., Ennis-King, J., Van Ruth, P., & Hillis, R. (2010). Geomechanical analysis of the Naylor Field, Otway Basin, Australia: Implications for CO_2 injection and storage. *International Journal of Greenhouse Gas Control, 4*(5), 827–839.

Vilarrasa, V., Carrera, J., & Olivella, S. (2013). Hydromechanical characterization of CO_2 injection sites. *International Journal of Greenhouse Gas Control, 19,* 665–677.

Ward, W. C., & McDonald, K. C. (1979). Nubia Formation of central Eastern Desert, Egypt—Major subdivisions and depositional setting. *AAPG Bulletin, 63*(6), 975–983.

Winter, D. A., & King, B. (1991). The West Sole Field, Block 48/6, UK North Sea. In: I.L. Abbotts (Ed.) United Kingdom Oil and Gas Fields, 25 Years Commemorative Volume. *Geological Society, London, Memoir, 14*, 517–523. https://doi.org/10.1144/GSL.MEM.1991.014.01.65.

Younes, A. I., & McClay, K. (2002). Development of accommodation zones in the Gulf of Suez-Red Sea rift Egypt. *AAPG Bulletin, 86*(6), 1003–1026.

Zhang, J. (2011). Pore pressure prediction from well logs: Methods, modifications, and new approaches. *Earth- Science Reviews, 108*(1–2), 50–63.

Zhang, J. (2013). Borehole stability analysis accounting for anisotropies in drilling to weak bedding planes. *International Journal of Rock Mechanics and Mining Sciences, 60,* 160–170.

Zhang, Y., & Zhang, J. (2017). Lithology-dependent minimum horizontal stress and in-situ stress estimate. *Tectonophysics, 703–704,* 1–8.

Zoback, M. D. (2007). *Reservoir Geomechanics*. California: Stanford University.

Zoback, M. D., & Zinke, J. C. (2002). Production-induced normal faulting in the Valhall and Ekofisk oil fields. *Pure and Applied Geophysics, 159,* 403–420.

Zoback, M. D., & Healy, J. H. (1984). Friction, faulting and 'In-Situ' stress. *Annals of Geophysics, 2*(6), 689–698.